PERGAMON

Journal of Structural Geology 25 (2003) 737–748

JOURNAL OF STRUCTURAL GEOLOGY

www.elsevier.com/locate/jstrugeo

Three-dimensional retro-deformation of the Lechtal Nappe, Northern Calcareous Alps

David C. Tanner*, Jan H. Behrmann, Horst Dresmann

Geologisches Institut, Universität Freiburg, Albertstraβe 23b, D-79104 Freiburg, Germany

Received 2 May 2001; accepted 1 May 2002

Abstract

We determine the amount of shortening, depth of detachment and the style of deformation of the Lechtal Nappe, the largest nappe within the Northern Calcareous Alps (German/Austrian border), by three-dimensional retro-deformation analysis of ca. 40 km^2 area. A three-dimensional model was constructed by splining lines from eight N–S cross-sections, spaced E–W at ca. 4 km intervals, to define fault geometrics and seven stratigraphic layers within the Permo-Triassic to Cretaceous strata. The modelled volume has four main thrusts which link to a common detachment at 2–5 km depth. Three-dimensional fault displacements and heaves were determined using Allan diagrams. The algorithms fault-parallel flow and flexual-slip unfolding were used to restore northwards movement on the thrusts and folding of beds over thrust planes, respectively. Minimum shortening estimates vary, from east to west, from 25 to 42% (typical error 6%), but additional shortening in the west is due only to folding.

Keywords: Northern Calcareous Alps; Lechtal Nappe; Three-dimensional retro-deformation; Structural restoration

1. Introduction

The Northern Calcareous Alps (NCA) belong to the Eastern Alps (sensu Tollmann, 1963) of Central Europe. The Eastern Alps are composed of the following geological units, from north to south:

1. German Molasse Basin. A thick prism of Oligocene marine to freshwater sediments. The unit was partially deformed by the advancing Alps. Molasse sediments underlie the nappe pile at least to the NCA.
2. Helvetic and Ultrahelvetic Nappes. Calcareous and other sedimentary rocks contained in nappes sliced up by thrusts; derived from zones between Penninic (i.e. belonging to the European crust) basement massifs.
3. Flysch Zone. Mostly Cretaceous–Eocene deep-water turbidites, which were deposited on the stretched European Margin (Oberhauser, 1968).
4. NCA. see below.
5. Graywacke Zone and Lower Austroalpine Units. This zone contains Austroalpine strata which was exposed to low-grade metamorphism during the Caledonian and Variscian Orogenies. It consists of Paleozoic limestones, greywackes, slates, phyllites, and other metamorphites.
6. Tauern Window. This is a tectonic window within the Austroalpine nappes which reveals basal Penninic units below.

The NCA formed the leading edge of the Adriatic Plate as it collided with the European Plate, causing the Alpine Orogeny (Tollmann, 1976; Ring et al., 1989). The youngest sediments of the Flysch Zone date the maximum age of thrusting of the NCA over the Helvetic Zone at 53 Ma (Schnabel, 1992). The western NCA consists of three major nappes (from N to S), the Allgäu, Lechtal and Inntal Nappes, the largest of which is the Lechtal Nappe. All three nappes contain equivalent Permo-Triassic to Cretaceous strata.

The aim of this work was to three-dimensionally retro-deform (i.e. remove in reverse) the internal, macro-scale, thrust and fold-related deformation of the Lechtal Nappe, within an area ca. 40×40 km^2 between Munich and Innsbruck, straddling the political border between Germany and Austria (Fig. 1).

* Corresponding author. Presently at: GeoForschungsZentrum Potsdam, Telegrafenberg, D-14473 Potsdam, Germany. Tel: +49-331-288-1306; fax: +49-331-288-1370.

E-mail address: tanner@gfz-potsdam.de (D.C. Tanner).

0191-8141/03/$ - see front matter © 2002 Elsevier Science Ltd. All rights reserved.
PII: S0191-8141(02)00057-3

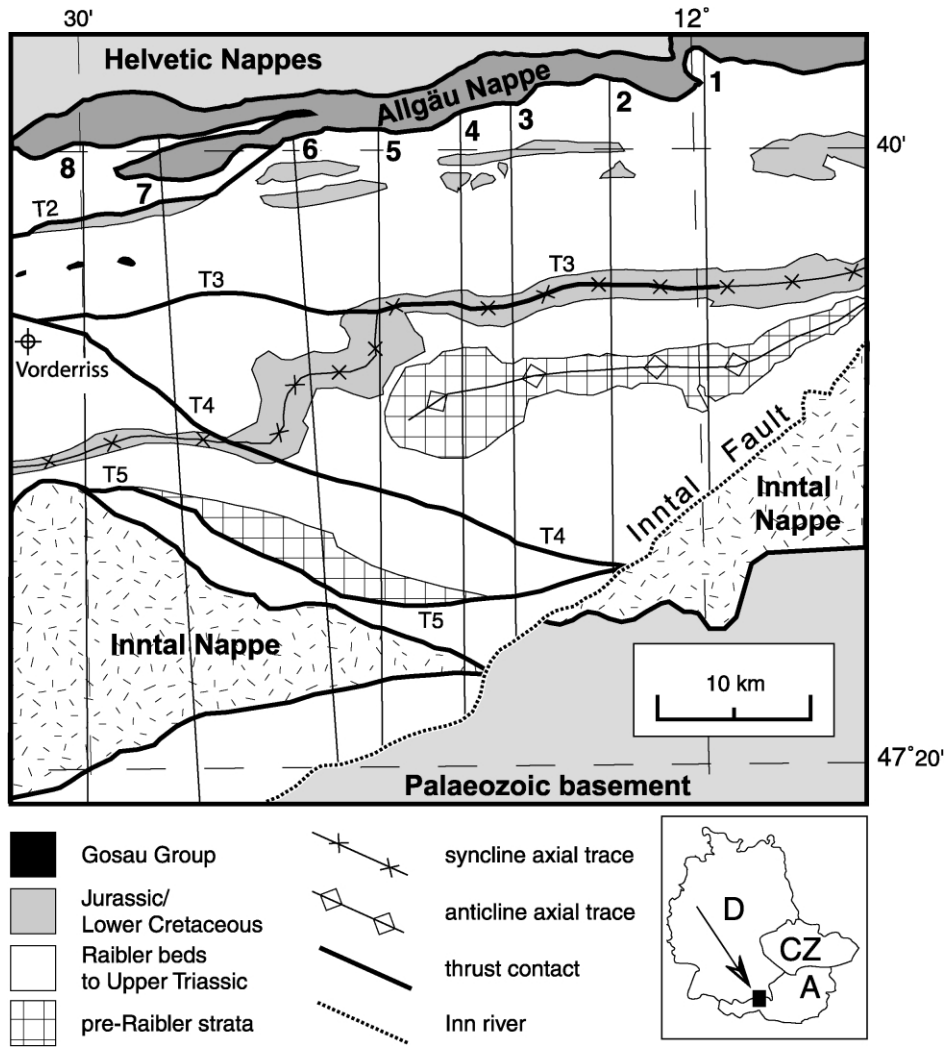

Fig. 1. Geological map of the studied area of the western NCA showing simplified stratigraphic units and traces of major fold axes. Thick black lines are thrust contacts (numbered as in text T2–T5, where applicable); stratigraphic contacts are thin black lines. Traces of cross-sections used to construct the 3D model are numbered 1–8. Vorderriss—Vorderriss borehole. D, A, CZ—Germany, Austria, Czech Republic, respectively.

2. Geological background of the western NCA nappes

All three nappes of the western NCA contain a continuous sequence of Permo-Triassic to Lower Cretaceous strata (Fig. 2). The basement of parts of the NCA is assumed to be the Graywacke Zone (Schramm, 1979); this contact is exposed on the southern side of the Inn River (see Fig. 1). The Mesozoic strata were deposited on the northwestern margin of the Tethys Ocean (Gawlick et al., 1999). The main stratigraphic unit of the area is the Norian Hauptdolomit (HD), a massive, coarsely-laminated, dolomite body (Zankl, 1967; Fruth and Scherreiks, 1984), that is between 700 and 2500 m thick.

The western NCA was subject to no more than anchimetamorphism (i.e. less than 200 °C), although illite data has shown the metamorphism of the Inntal Nappe is slightly higher than the Lechtal and Allgäu Nappes (Kralik et al., 1987).

The Upper Cretaceous Gosau Group (Figs. 1 and 2) consists of coarse conglomerates, sandstones, marls and limestones (Sanders, 1998) that lie unconformably on older, folded strata. It was tilted during the later stages of Alpine Orogeny (Faupl et al., 1987; Wagreich, 1992, 1995; Wagreich and Faupl, 1994; Ortner et al., 1999). In contrast, a significant amount of the deformation of the NCA occurred during the Late Eocene to Late Miocene (see discussions in Eisbacher and Brandner (1996), Linzer et al. (1997) and Peresson and Decker (1997)). Various authors have proposed slightly different kinematic systems to explain the development of the NCA and the Eastern Alps (e.g. Eisbacher et al., 1990; Peresson and Decker, 1997). Three main phases of deformation are evident:

1. Late Cretaceous NW-directed compression,
2. Early Tertiary N-directed compression, and
3. lateral extrusion from the Middle Miocene until present.

The main stage of thrusting within the NCA and the

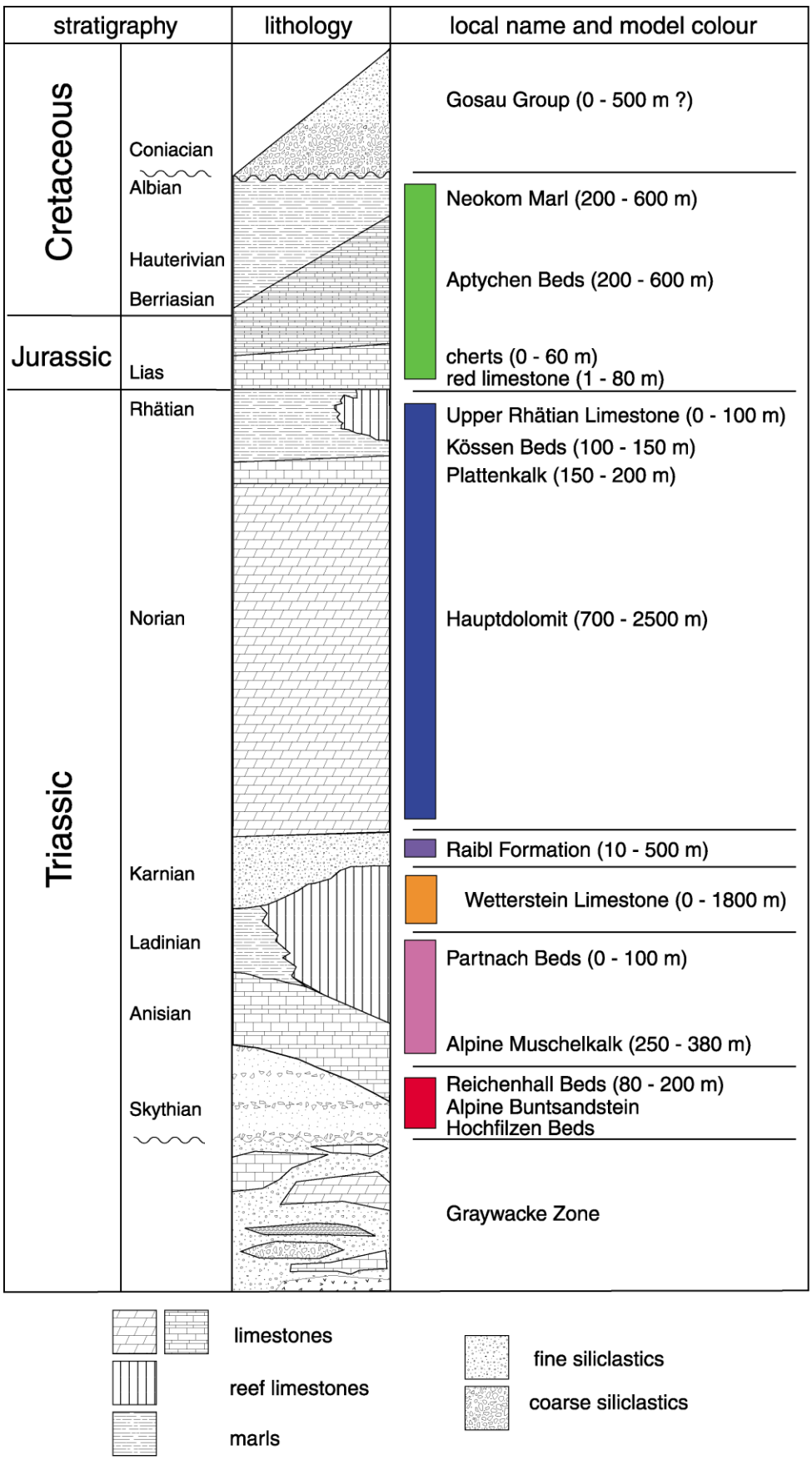

Fig. 2. Generalized stratigraphy of the NCA nappes. Coloured bars represent stratigraphic layers and their colours used throughout this work. Not to scale, as thicknesses vary intensely.

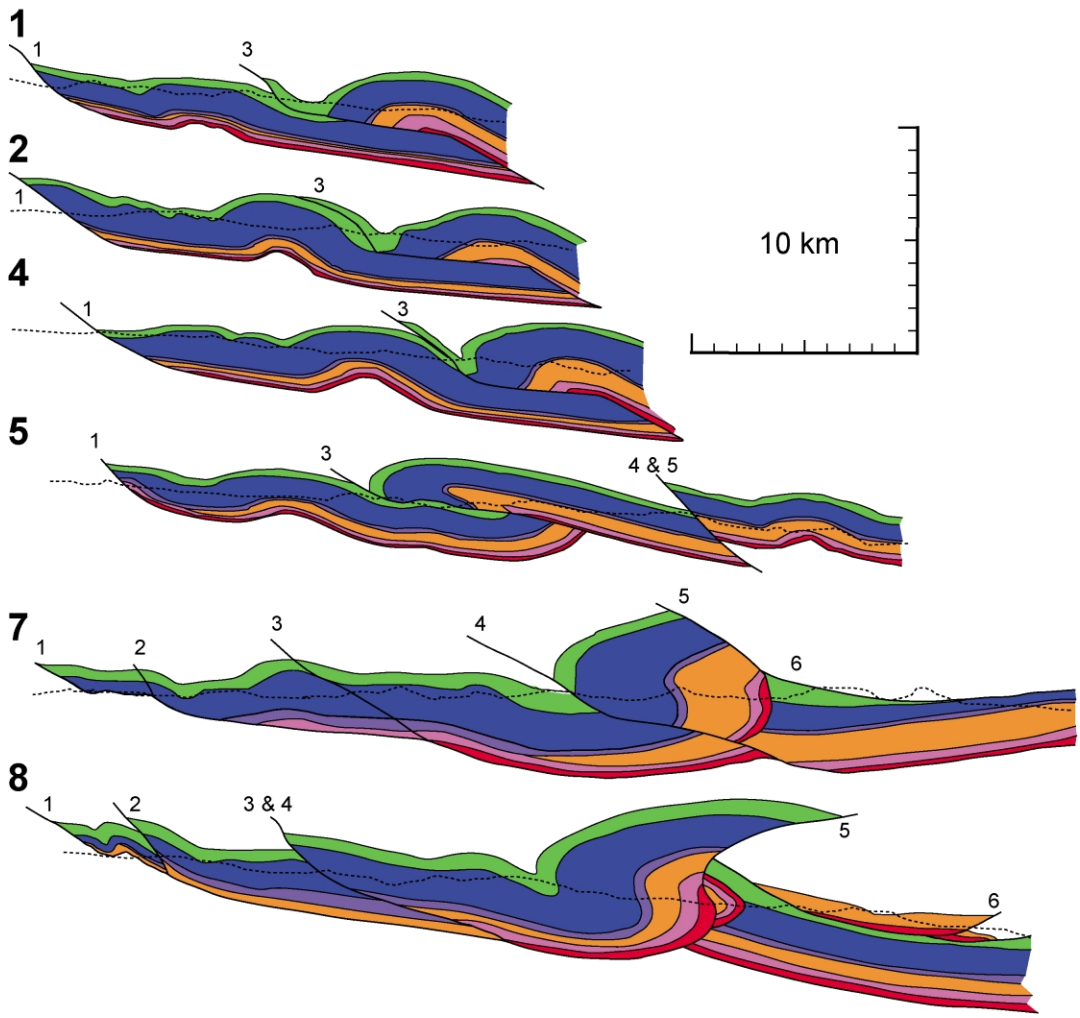

Fig. 3. Three-dimensional, parallel view (from WNW, 30° above horizontal) of six of the eight geological cross-sections (sections 3 and 6 omitted for clarity) of the LN used in this work, in true geographical position. Faults are thick black lines, present topography is fine-dashed black line. Stratigraphic colours as in Fig. 2. The southern edge of all sections is the near-vertical Inntal Fault.

Lechtal Nappe belongs to the second phase. A complicated system of changing stress regimes during the Miocene was documented by Peresson and Decker (1997), and this was mainly responsible for strike-slip movement during lateral extrusion. One such late feature is the Inntal Fault (Fig. 1), which has evidence of sinistral strike-slip movement since the Oligocene (Eisbacher and Brandner, 1996; Ortner et al., 1999), and forms the present southern boundary of the Lechtal and Inntal Nappes. The Inn River (Fig. 1) follows the trace of this fault.

3. Three-dimensional modelling

3.1. Construction of a 3D model of the LN

We constructed our model with the 3D-modelling software *3D-Move* (© Midland Valley Exploration Ltd). Eight cross-sections were constructed through the LN (Fig. 3; see Fig. 1 for location), based on geological maps (Schmidt-Thomé, 1953; Ganss and Doben, 1984; Eisbacher and Brandner, 1996) and from the 6 km deep Vorderriss borehole (Bachmann and Müller, 1981) (Fig. 1). The cross-sections were constructed from N to S, from the leading edge of the LN to the Inntal Fault. Faults were constructed at depth using two-dimensional line-balancing techniques. Above the topography, hanging-wall blocks were constructed using the principle of minimum displacement (Woodward et al., 1989).

For modelling, the stratigraphy of the LN is problematic because in nearly all strata there are strong lateral facies variations and rapid changes in bed thickness. Therefore it was not possible to produce a model with the classic undeformed template method (e.g. Woodward et al. 1989). Instead, bed thicknesses were derived from surface outcrops as much as possible and this data was used to predict beds at depth. Western sections could be correlated with thicknesses found in the Vorderriss borehole (Bachmann and Müller, 1981). This led to maximum errors in bed thickness of approximately 10%, depending on the subcrop length, but did not affect bed length.

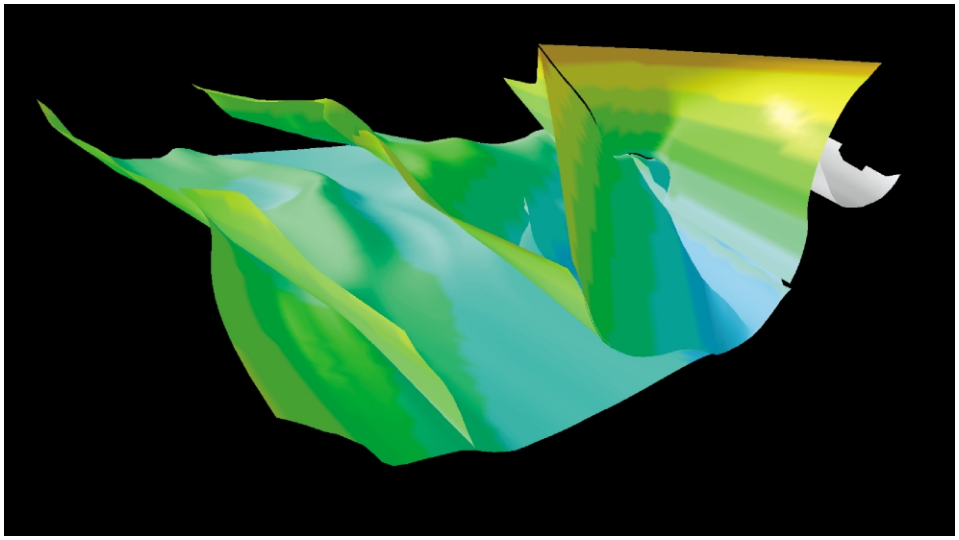

Fig. 4. Three-dimensional perspective view (from WNW, 15° above horizontal) of thrusts within the LN and the Inntal Nappe basal detachment. Note fold in the basal detachment caused by duplexing of the Allgäu Nappe (centre left). Thrusts 1–5 are colour-coded by depth every 500 m. Eastern light. Model is ca. 40 km wide (E–W).

To produce three-dimensional surfaces (irregular triangular grids in *3D-Move*), lines from each cross-section were joined together using the 'b-spline' technique (Forsey and Bartels, 1988). Faults were constructed first, and then stratigraphic surfaces within the fault blocks. The grid spacing was approximately 500 m. Therefore the surfaces, faults or stratigraphic, contain real data points from the maps at a spacing of 4 km in the E–W direction and 1 km in the N–S direction (this varies from surface to surface, depending on stratigraphic position). 2D constrained points are spaced at 4 km in the E–W direction and 250 m in the N–S direction. Consequently, approximately 80% of the vertices of the surfaces were generated by the splining technique.

3.2. Description of the 3D-model of the LN

In the following section we describe in detail the geometry of the model. We also correlate the model structures with previously-mapped structures. The LN has a northward-tapered wedge form, with a south-dipping basal detachment (Fig. 4). The detachment varies in dip between 5 and 25° and ramps up at the front of the nappe at an angle of 40–60°. The detachment has a maximum depth below the present topography of 4.1 km in the east and 5.2 km in the west. Four internal thrust faults were recognized (T2–T5; Fig. 3); T1 is the front of the LN. In the west of the area, the basal detachment is folded into the footwall syncline of T3.

Note also the small anticline in the detachment (Figs. 3 and 4), caused by duplexing in the lower Allgäu Nappe. The fold strikes E–W in the east, but turns to strike NW–SE in the middle of the area, where it dies out. The eastern structure of the LN (Fig. 3; sections 1 and 2) is dominated by a single thrust (T3—Achental Thrust; Eisbacher and Brandner, 1996). This fault has an angle of about 30° through the HD and lower strata, but flattens out in the footwall Jurassic. The hanging wall of T3 has developed into a large ($\lambda = 10$ km) hanging-wall anticline (Unutz Anticline; Eisbacher and Brandner, 1996). This anticline is near-symmetrical in the east, but becomes more north-vergent and tighter towards the west (Fig. 3). In addition, as the asymmetry of the hanging-wall anticline increases westwards, a footwall syncline (Thiersee Syncline; Eisbacher and Brandner, 1996) is developed. Footwall cutoff angles of about 30° are maintained because T3 becomes flatter towards the west.

In the middle of the model (Fig. 3; sections 4 and 5), a steeper-dipping (40–50°) thrust (T4—Eben Thrust; Eisbacher and Brandner, 1996) develops, raising the base of the nappe to less than a kilometre beneath the present topographic surface.

On the western side of the modelled area (Fig. 3; sections 5, 7 and 8) T4 becomes flatter, and a back thrust (T5—Eng Backthrust; Eisbacher and Brandner, 1996) develops between sections 6 and 7. T5 is partly overturned, so that it presently dips both between 40° S and 35° N. At the base of T5 in section 8 (Fig. 3), a small horse block of pre-HD stratigraphy is presently cut by the topography. Note T5 also displaces the Inntal Nappe by ca. 2.5 km. Between T4 and T5 a syncline is developed (Karwendel Syncline; Eisbacher and Brandner, 1996), which also folds the basal detachment.

The Inntal Nappe is shown in sections 7 and 8. Further to the west, this nappe extends for some tens of kilometres (Eisbacher and Brandner 1996). The Inntal Nappe basal detachment is sub-horizontal to bowl-shaped, dipping both moderately flat north and south in section 8. Small back thrusts are common on the trailing edge. Even from the limited outcrop, we estimate the Inntal Nappe has the same stratigraphy as the LN, but thicknesses are much reduced (except the WK, which is still over 600 m thick).

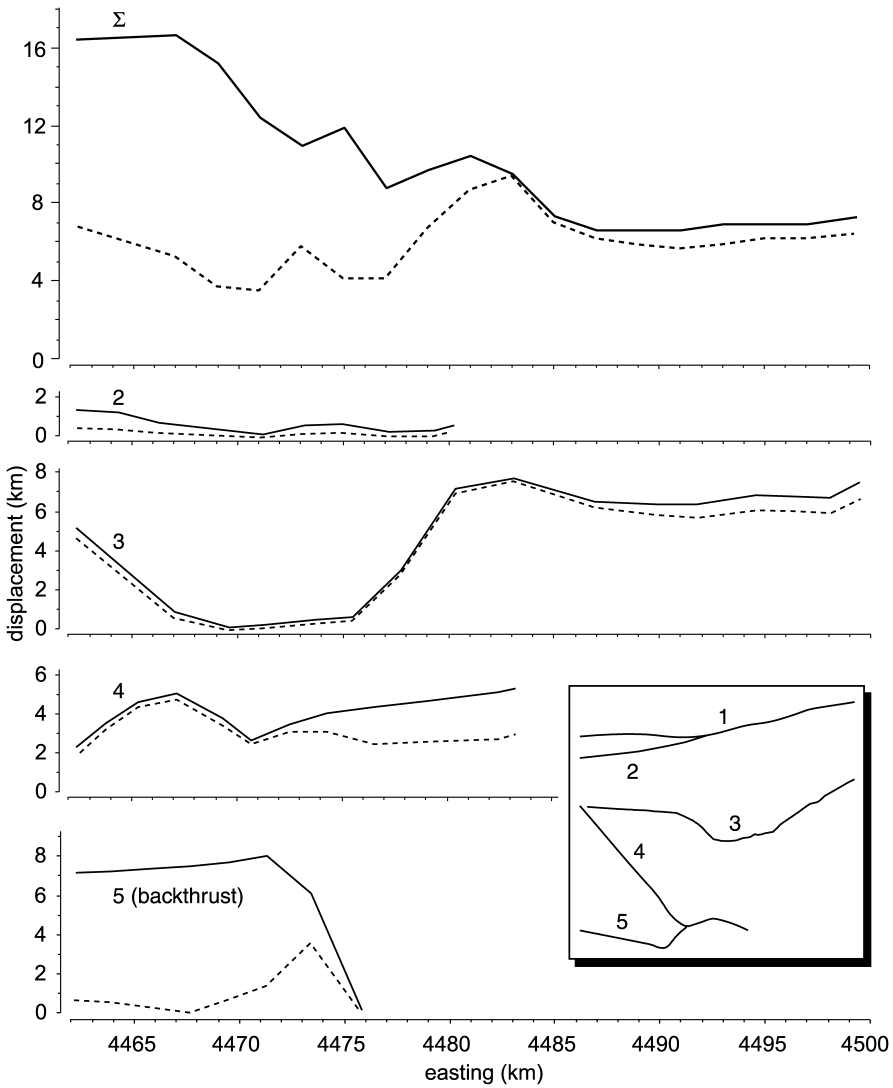

Fig. 5. Strike variation in fault slip (solid line) and heave (dashed line) of the base HD stratigraphic surface as determined by 'Allan mapping' (see text for description). Σ—total displacement on faults. Insert shows fault traces at 1 km above sea level.

3.3. Fault displacement and heave

Displacements and heave caused by T2–T5 were determined in *3D-Move* using 'Allan mapping' (Allan, 1989). In this method, chosen stratigraphic surfaces in the foot- and hanging-wall are projected (with their final dip) onto the fault plane in three-dimensions. The displacement vector was determined along the fault surface between the foot- and hanging-wall cutoffs, along the intersection with a vertical plane (in this case striking N–S, since the kinematics of the fault movement was N–S).

In general, in the east until easting 4485, total fault displacement is constantly 8 km, all of which is on T3 (Fig. 5). West of easting 4485, total displacement increases steadily up to 16 km, but this is distributed on T2–T5. Along strike, approximately at the branch point of T4 and T5, T3 displacement decreases sharply (within 6 km along strike) to less than 1 km. The along-strike westward gain in displacement of T5 is similarly impressive, gaining 8 km displacement in 5 km along strike westward from easting 4476.

The amount of heave (with respect to the displacement) in Fig. 5 demonstrates the flat nature (apparent angle of the fault, not dip, because the transport direction is not always perpendicular to the strike of the faults) of T2–T4 and the steep nature of T5. Note also how T4 becomes steeper to the east. Interestingly, total fault heave is approximately constant (approximately 6 ± 3 km), in the east/west direction.

4. Retro-deformation

4.1. Algorithms

4.1.1. Fault parallel flow

Egan et al. (1999) describe the algorithm 'fault-parallel flow' (FPF). Firstly, slip paths for all vertices in the

Table 1
Chronological ordered (1 = youngest) deformation stages of the Lechtal Nappe and retro-deformation method and parameters. FSU—flexual slip unfolding, FPF—fault parallel flow

No.	Stage	Retro-deformation		
		Method	Details	Kinematics
1	Duplexing of the Allgäu Nappe folds the LN from below	FSU	Pin plane set along fold axial plane	NNE–SSW
2	Thrusting on T2	FPF	Along-strike displacement from Allan diagram	S'ward
3	Thrusting movement on T3 (formation of hanging-wall anticline)	FPF	⋮	⋮
4	Thrusting movement on T4	FPF	⋮	⋮
5a	Thrusting movement on T5 (back/forward thrust and footwall syncline)	FSU	For all objects north of T5. Pin plane set along Karwendel Syncline axial plane	N–S
5b	⋮	FSU	For all objects south of T5. Pin plane set on T5	N–S

hanging-wall are determined in the direction of displacement. Consequently, vertices move along parallel lines over the three-dimensional surface of the fault, not perpendicular to the fault plane. Therefore the method can be considered to use plane strain. To accommodate changes in fault (apparent) dip (in the direction of displacement), dip domains are defined from the fault surface extending into the hanging-wall, bounded by lines bisecting the change in fault dip (see Appendix A). Travelling over a dip domain boundary will change the cutoff angle of, and strain within, lines and surfaces. This can be corrected by a certain amount of simple shear, parallel to the fault surface and the displacement direction (see Appendix A for details).

4.1.2. Flexual slip unfolding (FSU)

This algorithm is useful not only for removing folding, but also deformation caused by faulting, because it maintains (though only in the transport direction) bed length and bed area (cf. Suppe, 1983; Gratier et al., 1991). A template bed is restored to a target surface or horizontal and, if required, other objects can be passively translated by the same vectors as the template. A pin surface, the intersection of which with the template defines the points on the template and passive surfaces along which no slip can take place, may be constructed in three-dimensions.

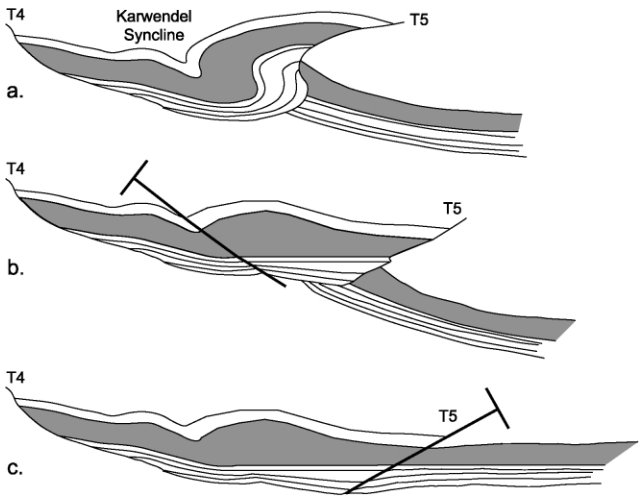

Fig. 6. Application of the FSU method, demonstrated here for retro-deformation of the Karwendel Syncline and the folded backthrust (T5) in section 8. (a) Present deformed situation. (b) Pin line set along fold axial trace of the Karwendel Syncline. The base of HD was chosen as the active layer, all other layers in the fault block are passive. Note orthogonal thicknesses are maintained. (c) Pin line set along T5. Base HD is brought horizontal, all other layers are passive.

4.2. Method

From observations of the three-dimensional model and an analysis of cross-cutting structures, we ascertained that there were no out-of-sequence thrusts, and the most probable geological scenario was one of a forward-propagating thrust system within the LN, even though the LN was probably thrust over the Allgäu Nappe during the Cretaceous (Gaupp, 1982; May and Eisbacher, 1999). Therefore to remove the deformation stages in reverse order, the duplex folding of the LN detachment was removed first and then movement on T2–T5.

A combination of FSU and FPF was used to retro-deform the folds and thrust of the LN, respectively (Table 1). Unfortunately it was impossible to use FPF for T5 because of its partially overturned nature which was still present (even if to a lesser degree; see below) after retro-deformation of T4. Instead FSU was used to restore the base HD to a horizontal plane twice (also allowing for along-strike displacement variation in the third dimension): once on both sides of the T5 fault plane (Table 1). This is shown graphically in two dimensions in Fig. 6.

5. Results

Fig. 7 shows eight cross-sections through the retro-deformed 3D model. T4 and T5 have both been steepened by retro-deformation shear on T3 (ignore the trace of T4

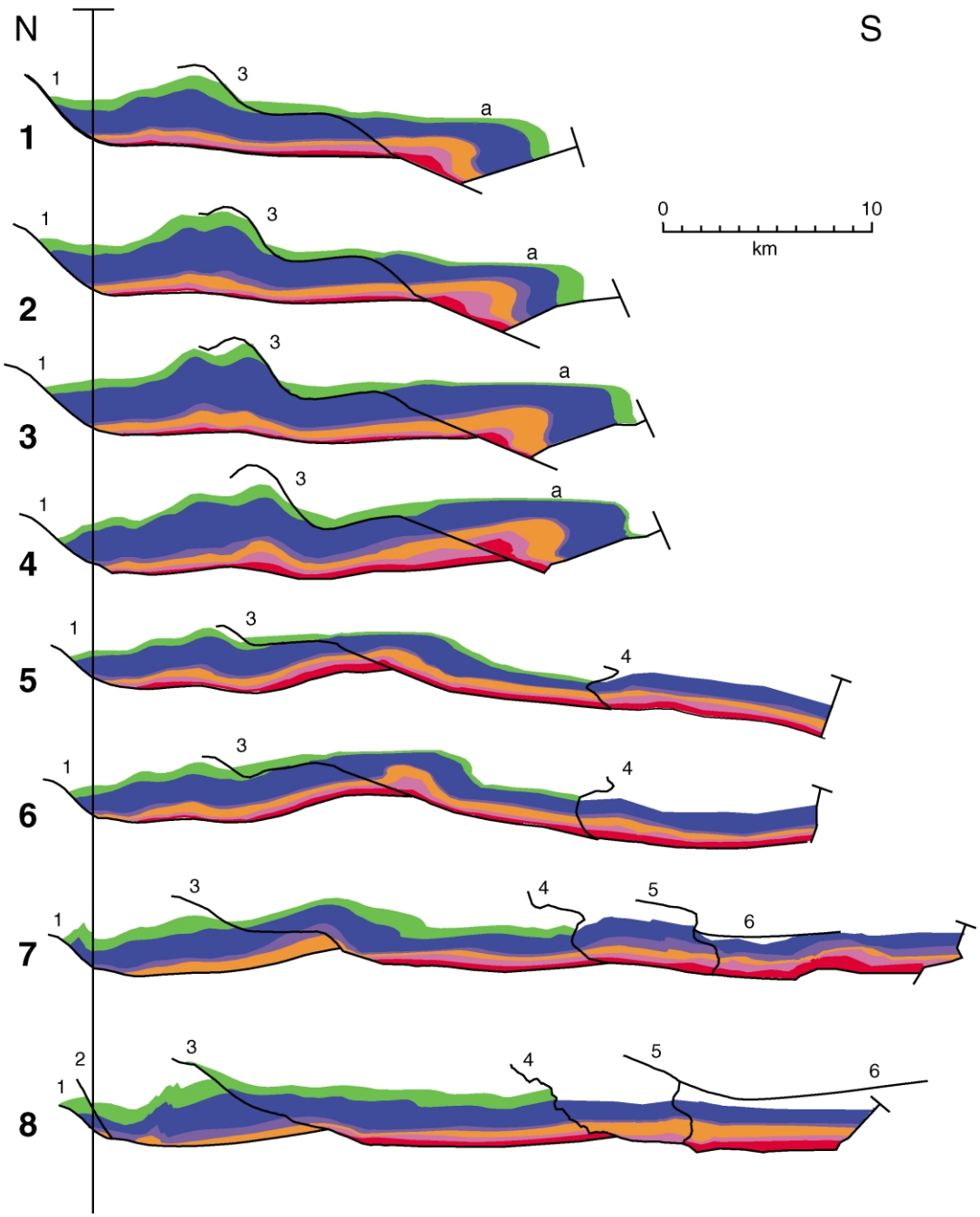

Fig. 7. Direct parallel (2D) view of eight cross-sections through the 3D-model of the LN after retro-deformation. Sections are so arranged that they have a mutual northern pin-line (on base HD). Note that, although the first section is parallel to the previous first section, others are spaced at intervals of 4 km westwards, so that section 8 here is ca. 2 km east of previous section 8. Faults are black and numbered as before. Stratigraphic colours as in Fig. 2. See text for explanation of the fold at a.

above the Cretaceous, since this was not constrained). Although such steep angles would normally be unacceptable in restoration (e.g. Woodward et al., 1989), many of the faults of the NCA are steep (ca. 60–70°), at least in places such as within the HD (see T1 and the upper part of T3; also Eisbacher and Brandner, 1996).

Errors and mismatches were left in Fig. 7 to additionally demonstrate the problems and shortcomings of the retro-deformation algorithms and methods (see below). Shortening values were taken from Fig. 7 (Table 2). N–S shortening varies between 25 and 42%, increasing generally from east to west.

6. Discussion

6.1. Along-strike change in tectonic shortening of the LN

Because the Inntal Fault removes more of the sections in

Table 2
Horizontal shortening values (of the base HD) for each cross-section. l_o—original length (after retro-deformation), l_1—present length (before retro-deformation), Δl—change in length

Section	l_o (km)	l_1 (km)	Δl (km)	$(\Delta l/l_o) \times 100$ (%)	Error[a] (%)
1	27.3	18.7	8.6	31.5	5.2
2	27.4	19.3	8.1	30.0	10.0
3	31.0	22.3	8.7	28.1	9.6
4	30.9	23.0	7.9	25.6	12.9
5	57.9	34.0	23.9	41.3	2.8
6	59.6	34.5	25.1	42.1	5.7
7	65.6	39.6	26.0	40.0	3.0
8	64.7	41.0	23.7	36.6	5.4

[a] The amount of underestimation of shortening of the HD when compared with 2D line balancing.

the east than in the west, direct comparison of tectonic shortening is difficult. However, the displacement relationship of T3 to T4 and T5 (Fig. 5) suggests that T4 does die out eastwards. Moreover, because total fault heave is nearly constant through the area, higher shortening values (see Table 2; column 5) must represent additional shortening by folding. Therefore it is the tectonic shortening by folding which increases towards the west, while thrust heave remains constant.

6.2. Comparison with previous (2D) models

Dresmann (2000) retro-deformed two cross-sections of the LN (approximately sections 3 and 4 in this work) and the Allgäu Nappe. He estimated the internal shortening in the eastern and western sections to be 23–24% and 37–39%, respectively. Total shortening across both nappes was estimated at 44%. This is far less than the estimates of Linzer et al. (1995) and Eisbacher et al. (1990), who from three sections (80 km east and 140 km west, and 85 km west of this working area, respectively), estimated tectonic shortening to be 65 and 54%, and 60%, respectively. However these authors included the Inntal Nappe, which was not included here; firstly because there is very little outcrop (N–S or E–W) of the Inntal Nappe in the modelled area, and secondly because the Inntal Fault removed the trailing edge of the LN. It should be noted that the same authors did not consider T5 of this work.

There is, however good agreement about the depth of detachment. Linzer et al. (1995) and Eisbacher et al. (1990) both estimated the basal detachment to be 2.4–2.8 km in the north and 4.6 km in the south of the NCA.

6.3. Applicability of retro-deformation methods and associated errors

A number of sources of error are clearly seen in Fig. 7. These include:

1. Strong layer-parallel shearing of the model in sections 1–4. To restore the tight to isoclinal, recumbent, hanging-wall anticline of T3, 60° shear ($\gamma = 1.7$) was applied during stage 3 of the retro-deformation. This is seen in the angle of the originally vertical marker-pin at the southern end of these sections. A shear strain of 1.7 was estimated to be the average amount of shear to compensate for the net concave-down fault segments of Thrust 3 (see Appendix A for the necessity of shear compensation of fault topography). The retro-deformation of the hanging-wall fold was only moderately successful since a residual fold (Fig. 7; fold a) is still present.
2. Mismatch of beds. Restoration was applied to the base HD, so other beds do not necessarily meet across faults. Both retro-deformation methods do not conserve bed volume or even bed cross-sectional area other than in the transport direction. This is the greatest source of the bed mismatch. Typically it is less than a few hundred metres.
3. Strata thickness variation. This is mostly real, i.e. the stratigraphic units *do* undergo large thickness changes in all directions (see below). However for the same reason as in 2, bed volume or area may have changed especially in areas of high strain (e.g. in fold a; Fig. 7).

Nevertheless, flexual-slip methods for thrust and fold belts are preferable to inclined-shear methods (Williams et al., 1997). The latter are better for extensional fault systems or hanging-wall strata without bedding (e.g. Tanner et al., 1998). This work shows that FPF, with the application of additional shear, can restore upright to inclined hanging-wall folds, but not recumbent folds, since overturned beds cannot be properly moved. FPF is also an advance over the 2D flexual-slip method of Suppe (1983), in as far as this requires an exact ramp/flat fault geometry.

6.4. Structural style and stratigraphic thickness

Many of the stratigraphic layers in the modelled area vary greatly in thickness, especially the HD and WK, but also the Raibl beds and Jurassic strata (Figs. 3 and 7). Our model, substantiated by surface data, shows that in general the HD increases in thickness from less than 1 km at the front of the LN to 1.5–2.5 km in the middle of the area. This effect is much more marked in the west. Towards the south, the HD thickness decreases again, especially in sections where it is thickest in the middle of the area (cf. Section 7). The WK has a thickness of ca. 300–800 km in the eastern and middle sections, wedging out towards the front of the nappe. In the western sections, this effect is much more pronounced, where the WK wedges out sharply in less than 5 km.

These stratigraphic thickness variations are largely responsible for the structural style of this area, for example:

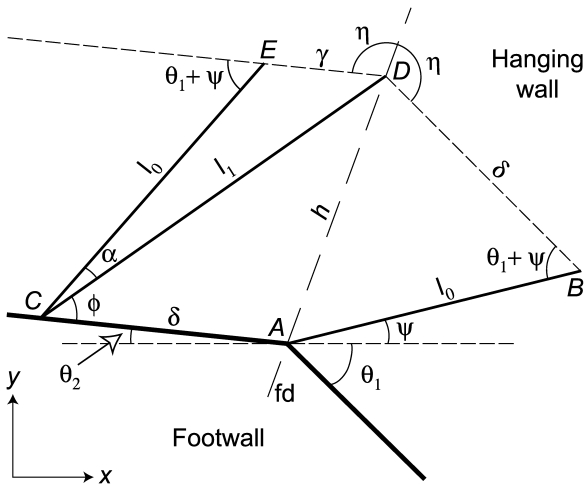

Fig. 8. Fault-parallel flow. The line $A-B$ is displaced along fault-parallel flow lines (fine-dashed line and fault (thick line)) to the line $C-D$. Consequently to remove strain and restore cutoff angle (i.e. line $C-E$), fault-parallel shear (γ) is required. See text for details. fd—flow deflector.

1. The LN detachment ramps up where the HD is thinnest and the WK is typically not present. In this area, thrust splays from the detachment are common.
2. The foot- and hanging-wall folds of T3 and T4 are best developed (tighter, but with a greater wavelength) where the HD is thickest.
3. We suggest the major folds (Thiersee and Karwendel Synclines) were caused by the inability of the thrusts (especially T3 and T4) to propagate through the HD, i.e. they represent fault-propagation folds.

7. Conclusions

A three-dimensional model of a 40×40 km^2 area of the LN, the largest nappe system of the NCA, was built from eight two-dimensionally line-balanced cross-sections. The model consists of four inter-nappe thrust faults which join a detachment at 2–5 km depth. A hanging-wall anticline is apparent above T3 and a footwall syncline is developed below T4. The foreland-stacking system was thrust northwards during the Mid Tertiary.

To retro-deform the model, deformation phases (1–5) were removed in reverse order with reverse kinematics. Retro-deformation was achieved using FSU and FPF. We make the following points:

1. Total fault heave is relatively constant along strike of the major structures, but total displacement increases from 8 to 16 km, from east to west.
2. Total shortening also increases from east to west; this is due to stronger folding on the western side of the model.
3. The algorithms were not able to completely restore all the deformation, especially the recumbent hanging-wall anticline of T3. Total error is as high as 13%, but typically less than 6%.
4. The structural style of the modelled area depends to a great extent on the thickness of the HD, which acts as a controlling layer.
5. Three-dimensional modelling produces lower estimates of shortening than two-dimensional methods. This is due mainly to the tight, detailed constraints involved in three-dimensional modelling, e.g. along-strike displacement variation must be accounted for.

Acknowledgments

This work was part of the DFG (German Research Council) TRANSALP program and we acknowledge the receipt of a DFG research grant. Michael Wagreich and Mark Fischer are thanked for constructive and detailed reviews. Some of this work was part of H. Dresmann's Diplom thesis. We thank Midland Valley Exploration Ltd for support of their software program *3D-Move*.

Appendix A. Calculation of shear correction during fault parallel flow

Fig. 8 shows a fault consisting of a ramp and flat, which make the angles θ_1 and θ_2, respectively, with the horizontal. Movement over the fault is allowed along flow lines parallel to the fault (Fig. 8). The flow deflector bisects the angle made by the two fault segments, thus defining the boundary between two dip domains. The angle η is defined, for concave-down fault segments as:

$$\eta = 90^\circ + \frac{\theta_1 + \theta_2}{2} \tag{1}$$

(Egan et al., 1999). Consider a line $A-B$ within the first dip domain, which has a original dip of ψ. The cut-off angle is thus $\psi + \theta_1$. The original length of the line (l_o) is given using the sinus rule on the triangle ABD:

$$l_o = \frac{\delta \sin(90^\circ - 2\theta_2 + \psi)}{\sin(\eta - \theta_1 + \psi)} \tag{2}$$

similarly, the length h is:

$$h = \frac{\delta \sin(\theta_1 + \psi)}{\sin(\eta - \theta_1 + \psi)} \tag{3}$$

After displacement δ along the flow lines (Fig. 8), the line is defined by the points C and D, which have the following coordinates:

$$\begin{aligned}(x_C,\ y_C) &= (x_A + \delta\cos\theta_2,\ y_A + \delta\sin\theta_2)\\ (x_D,\ y_D) &= (x_B + \delta\sin(90^\circ - \theta_1),\ y_B + \delta\cos(90^\circ - \theta_1))\end{aligned} \tag{4}$$

The length of the line $C-D$ (l_1) is given, using the cosine

rule:

$$l_1 = \sqrt{\delta^2 + h^2 - 2\delta h\cos\eta} \tag{5}$$

and hence the extension (e) of the line is given as:

$$e = \frac{l_1 - l_o}{l_o} \tag{6}$$

The new cut-off angle (ϕ) is, using the sine rule, given as:

$$\phi = \sin^{-1}\left(\frac{h\sin\eta}{l_1}\right) \tag{7}$$

To maintain line length and cut-off angle, the line $C-D$ can be transformed by simple shear parallel to the flow lines of the second dip domain to the new line $C-E$. The co-ordinates of E are defined as:

$$(x_E,\ y_E) = (x_C - l_o\cos(\theta_1 + \psi - \theta_2),\ y_C - l_o\sin(\theta_1 + \psi - \theta_2)) \tag{8}$$

Using the sinus rule, the required shear (γ) is given as:

$$\gamma = l_o\frac{\sin\alpha}{\sin\phi} \tag{9}$$

Since $\alpha = \theta_1 + \psi - \phi$, it is possible to show that γ is directly proportional to η, ψ and δ by substituting Eqs. (1)–(7) into Eq. (9).

References

Allan, U.S., 1989. Model for hydrocarbon migration and entrapment within faulted structures. The American Association of Petroleum Geologists Bulletin 73, 803–811.

Bachmann, G.H., Müller, M., 1981. Geologie der Tiefbohrung Vorderriβ 1 (Kalkalpen, Bayern). Geologica Bavarica 81, 17–53.

Dresmann, H., 2000. Bilanzierung zweier geologischer Profile zwischen Tegernsee (Deutschland) und Schwaz (Österreich). Unpublished Diploma thesis, University of Freiburg.

Egan, S.S., Kane, S., Buddin, T.S., Williams, G.D., Hodgetts, D., 1999. Computer modelling and visualisation of the structural deformation caused by movement along geological faults. Computers and Geosciences 25, 283–297.

Eisbacher, G.H., Brandner, R., 1996. Superposed fold–thrust structures and high-angle faults, northwestern Calcareous Alps, Austria. Eclogæ Geologicæ Helvetiæ 89, 553–571.

Eisbacher, G.H., Linzer, H.G., Meier, L., Polinski, R., 1990. A depth-extrapolated structural transect across the Northern Calcareous Alps of western Tirol. In: Jordan, P., Noack, T., Schmid, S., Bernoulli, D. (Eds.), The Hans Laubscher volume. Eclogæ Geologicæ Helvetiæ 83, pp. 711–725.

Faupl, P., Pober, E., Wagreich, M., 1987. Facies development of the Gosau Group of the eastern parts of the Northern Calcareous Alps during the Cretaceous and Paleogene. In: Flügel, H.W., Faupl, P. (Eds.), Geodynamics of the Eastern Alps, pp. 142–155.

Forsey, D.R., Bartels, R.H., 1988. Hierarchical b-spline refinement. Computer Graphics 22, 205–212.

Fruth, I., Scherreiks, R., 1984. Hauptdolomit; sedimentary and paleogeographic models (Norian, Northern Calcareous Alps). Geologische Rundschau 73, 305–319.

Ganss, O., Doben, K., 1984. Geologische Karte von Bayern 1:100,000, Blatt 665, Schliersee. Bayersiche Geologisches Landesamt, Munchen.

Gaupp, R., 1982. Sedimentationsgeschichte und Paläotektonik der kalkalpinen Mittelkreide (Allgäu, Tirol, Vorarlberg). Zitteliana 8, 33–72.

Gawlick, H.-J., Frisch, W., Vecsei, A., Steiger, T., Böhm, F., 1999. The change from rifting to thrusting in the Northern Calcareous Alps as recorded in Jurassic sediments. Geologische Rundschau 87, 644–657.

Gratier, J.-P., Guillier, B., Delorme, A., Odonne, F., 1991. Restoration and balance of a folded and faulted surface by best-fitting of finite elements; principle and applications. Journal of Structural Geology 13, 111–115.

Kralik, M., Krumm, H., Schramm, M., 1987. Low degree and very low degree metamorphism in the Northern Calcareous Alps and in the greywacke zone; illite, crystallinity data and isotopic ages. In: Fluegel, H.W., Faupl, P. (Eds.), Geodynamics of the Eastern Alps, pp. 164–178.

Linzer, H.G., Ratschbacher, L., Frisch, W., 1995. Transpressional collision structures in the upper crust; the fold–thrust belt of the Northern Calcareous Alps. In: Neubauer, F., Ebner, F., Wallbrecher, E. (Eds.), Tectonics of the Alpine–Carpathian–Pannonian region. Tectonophysics 242, pp. 41–61.

Linzer, H.G., Moser, F., Nemes, F., Ratschbacher, L., Sperner, B., 1997. Build-up and dismembering of the eastern northern Calcareous Alps. In: Neubauer, F., Cloetingh, S., Dinu, C., Mocanu, V. (Eds.), Tectonics of the Alpine–Carpathian–Pannonian region; II. Tectonophysics 272, pp. 97–124.

May, T., Eisbacher, G.H., 1999. Tectonics of the synorogenic 'Kreideschiefer basin', Northwestern Calcareous Alps, Austria. Eclogæ Geologicæ Helvetiæ 92, 307–320.

Oberhauser, R., 1968. Beiträge zur Kenntnis der Tektonik und Paläogeographie während der Oberkreide und dem Paläogen im Ostalpenraum. Jahrbuch der Geologischen Bundesanstalt Wien 111, 115–145.

Ortner, H., Brandner, R., Gruber, A., 1999. Kinematic evolution of the Inn Valley shear zone from Oligocene to Miocene. In: Szekely, B., Dunkl, I., Kuhlemann, J., Frisch, W. (Eds.), 4th Workshop on Alpine Geological Studies. Tuebinger Geowissenschaftliche Arbeiten. Reihe A, Geologie, Palaeontologie, Stratigraphie 52, pp. 192–193.

Peresson, H., Decker, K., 1997. The Tertiary dynamics of the northern Eastern Alps (Austria): changing palaeostresses in a collisional plate boundary. Tectonophysics 272, 125–157.

Ring, U., Ratschbacher, L., Frisch, W., Biehler, D., Kalik, M., 1989. Kinematics of the Alpine plate margin: structrual styles, strain and motion along the Penninic–Austroalpine boundary in the Swiss–Austrian Alps. Journal of the Geological Society, London 146, 835–849.

Sanders, D., 1998. Tectonically controlled Late Cretaceous terrestial to netric deposition (Northern Calcareous Alps, Tirol, Austria). Facies 39, 139–178.

Schmidt-Thomé, P., 1953. Geologische Karte von Bayern 1:100,000, Blatt 664, Tegernsee. Bayisches Geologisches Landesamt, München.

Schnabel, W., 1992. New data on the Flysch Zone of the Eastern Alps in the Austrian sector and new aspects concerning the transition to the Flysch Zone of the Carpathians. Cretaceous Research 13, 405–419.

Schramm, J.M., 1979. Bemerkungen zum Metamorphosegeschehen in klastischen Sedimentgesteinen im Salzburger Abschnitt der Grauwackenzone und der Nördlichen Kalkalpen. In: Tollmann, A., Kristan, T.E. (Eds.), Geologischer Tiefbau der Ostalpen. Mitteilungen der Oesterreichischen Geologischen Gesellschaft 71–72, pp. 379–384.

Suppe, J., 1983. Geometry and kinematics of fault bend folding. American Journal of Science 28, 684–721.

Tanner, D.C., Behrmann, J.H., Oncken, O., Weber, K., 1998. Three-dimensional retro-modelling of transpression on a linked fault system: the Upper Cretaceous deformation on the western border of the Bohemian Massif, Germany. In: Holdsworth, R.E., Strachan, R.A., Dewey, J.F. (Eds.), Geological Society, London, Special Publications 135, pp. 275–287.

Tollmann, A., 1963. Ostalpensynthese, Deuticke, Vienna.

Tollmann, A., 1976. Der Bau der Nördlichen Kalkalpen. Monographie der Nördlichen Kalkalpen, III, Deuticke, Vienna.

Wagreich, M., 1992. Subsidence history of the Gosau Group; why a model of Late Cretaceous simple extension does not work in the Northern Calcareous Alps. In: Anonymous (Ed.), ALCAPA; geological evolution of the internal Eastern Alps, Carpathians and of the Pannonian Basin. Terra Abstracts 4, pp. 69–70.

Wagreich, M., 1995. Subduction tectonic erosion and Late Cretaceous subsidence along the northern Austroalpine margin (Eastern Alps, Austria). In: Neubauer, F., Ebner, F., Wallbrecher, E. (Eds.), Tectonics of the Alpine–Carpathian–Pannonian region. Tectonophysics 242, pp. 63–78.

Wagreich, M., Faupl, P., 1994. Palaeogeography and geodynamic evolution of the Gosau Group of the Northern Calcareous Alps (Late Cretaceous, Eastern Alps, Austria). Palaeogeography, Palaeoclimatology, Palaeoecology 110, 235–254.

Williams, G.D., Kane, S.J., Buddin, T.S., Richards, A.J., 1997. Restoration and balance of complex folded and faulted rock volumes: flexural flattening, jigsaw fitting and decompaction in three dimensions. Tectonophysics 273, 203–218.

Woodward, N.B., Boyer, S.E., Suppe, J., 1989. An outline of balanced cross-sections: an essential technique in geological research and exploration. Short Course in Geology 6, 132pp.

Zankl, H., 1967. Die Karbonatsedimente der Obertrias in den nördlichen Kalkalpen. Geologische Rundschau 56, 128–139.